The Effects of Crosswind Flight on Rotor Harmonic Noise Radiation

Eric Greenwood*
Aeroacoustics Branch
NASA Langley Research Center
Hampton, VA

Ben W. Sim†
US Army Aviation Development Directorate – AFDD
Aviation & Missile Research, Development & Engineering Center
Research, Development and Engineering Command
Moffett Field, CA

ABSTRACT

In order to develop recommendations for procedures for helicopter source noise characterization, the effects of crosswinds on main rotor harmonic noise radiation are assessed using a model of the Bell 430 helicopter. Crosswinds are found to have a significant effect on Blade-Vortex Interaction (BVI) noise radiation when the helicopter is trimmed with the fuselage oriented along the inertial flight path. However, the magnitude of BVI noise remains unchanged when the pilot orients the fuselage along the aerodynamic velocity vector, "crabbing" for zero aerodynamic sideslip. The effects of wind gradients on BVI noise are also investigated and found to be smaller in the crosswind direction than in the headwind direction. The effects of crosswinds on lower harmonic noise sources at higher flight speeds are also assessed. In all cases, the directivity of radiated noise is somewhat changed by the crosswind. The model predictions agree well with flight test data for the Bell 430 helicopter captured under various wind conditions. The results of this investigation would suggest that flight paths for future acoustic flight testing are best aligned across the prevailing wind direction to minimize the effects of winds on noise measurements when wind cannot otherwise be avoided.

NOTATION

D_F	Fuselage parasite drag.
f_e	Effective flat plate drag area of the fuselage.
g	Gravitational acceleration.
h	Altitude above ground.
H	Rotor "hub" force.
R	Rotor radius.
t	Time.
V	Rotor free stream velocity.
V_{GND}	Helicopter ground-track (inertial) velocity.
V_{IAS}	Helicopter indicated airspeed.
w	Wind velocity.
W	Helicopter weight.
α_F	Fuselage angle of attack.
α_{TPP}	Rotor tip-path-plane angle of attack.
β_F	Fuselage sideslip angle.
β_I	Angle between free stream and inertial velocities.
γ	Flight path angle.
ρ	Air density.
μ	Main rotor advance ratio.
θ	Elevation angle relative to the horizon.
ψ	Azimuth angle relative to flight path.
ξ	Linear wind gradient magnitude.
Ω	Rotor rotational speed.

*Research Aerospace Engineer, eric.greenwood@nasa.gov

†Research Scientist, welchong.sim.civ@mail.mil

INTRODUCTION

Acoustic mission planning tools, such as the Rotorcraft Noise Model (RNM), (Refs. 1–3) develop and apply empirical models of helicopter external noise radiation to assess the annoyance or detectability of helicopter flight operations. Empirical noise models are used because they are able to provide accurate noise estimates quickly and at a relatively low computational cost. However, the process of collecting the acoustic data from which these models are constructed is complex. Typically, a specific model of helicopter is characterized by repeated flights of the helicopter over a ground-based linear array of microphones. During each flight, the helicopter remains in a steady flight condition following a straight-line flight path over the microphone array, shown in Figure 1.

As the helicopter passes over the microphone array, acoustic measurements are captured across a range of directivity angles with respect to single point on the helicopter, typically located at the main rotor hub. The method assumes that the helicopter's noise radiation characteristics can be represented in the far-field as a compact source and that this acoustic source does not vary over time because the helicopter's flight condition is nominally steady. Under these assumptions, ground-based noise measurements are normalized to a fixed distance away from the assumed compact source, accounting for spherical spreading and atmospheric absorption losses. This process forms an acoustic hemisphere representing the noise radiation characteristics of the helicopter for a particular flight condition. These hemispheres are frequently represented using a Lambert projection, shown in Figure 2 with coordinates aligned with the flight path and affixed to the horizon plane. The Lambert projection maps data from the surface of the hemisphere to a conic section which is unrolled for display in two dimen-
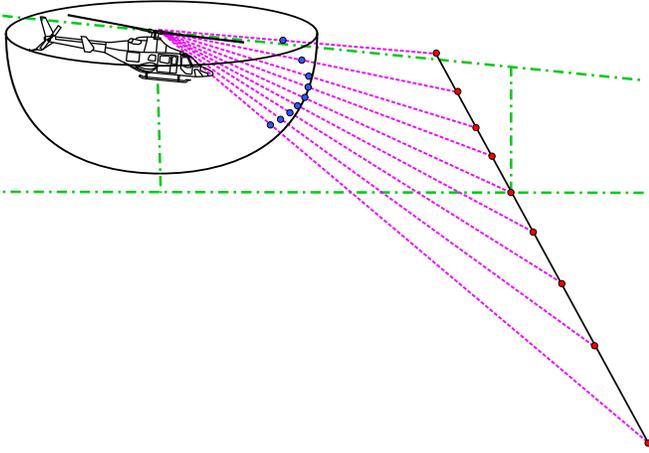
Fig. 1. Diagram of the process of building an empirical source noise hemisphere for a straight-line steady flight condition. Red points represent ground-based microphone locations and blue points the corresponding locations on the acoustic hemisphere surface.

sions. (Ref. 4) This projection is used because it minimizes the distortion in area of features when they are displayed in two dimensions, more accurately representing the relative important of features to the overall noise radiation of the helicopter. The acoustic hemisphere construction process is repeated for numerous flight conditions, typically varying airspeed and flight path angle, in order to develop a database of the helicopter noise radiation characteristics as a function of the steady operating condition. The result is a model of the helicopter noise radiation characteristics which can be applied to assess the acoustic characteristics of a proposed mission or flight plan.

During flight testing, low wind conditions are sought out, but it is rare that zero wind conditions can be obtained. Flight paths for source noise characterization measurements are typically aligned along the prevailing headwind direction, as is common in vehicle performance testing. However, winds oriented along the direction of propagation are known to have a strong effect on the propagation of sound from the source to the observers. (Refs. 5–7) On the other hand, the effects of wind normal to the propagation path are known to be relatively small, (Refs. 8,9) inducing small shifts in the observed directivity pattern. The relatively small effects of crosswinds are often neglected in propagation codes.

In addition to the effects on propagation, headwinds are known to affect the source noise characteristics of rotorcraft in flight. Near the ground, wind speeds tend to increase with altitude forming a wind gradient. Previous theoretical and experimental investigation has shown that during descending flight conditions, such as those where Blade-Vortex Interaction (BVI) noise occurs, the wind gradient induces a longitudinal acceleration on the helicopter as it flies at a constant airspeed. (Ref. 10) This longitudinal acceleration has the effect of changing the trim state of the vehicle, and hence the tip-path-plane angle of attack. This change in the tip-path-plane angle of attack is equivalent to a change in the flight path angle of the vehicle and has a strong effect on the radiated BVI noise. The effects
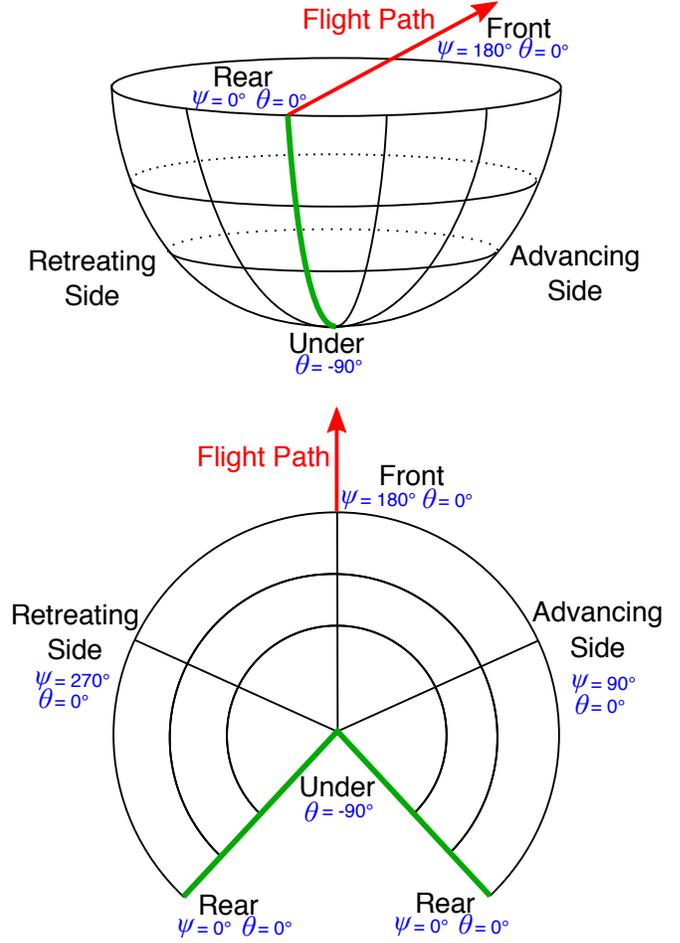
Fig. 2. Lambert projection of an acoustic hemisphere.

of crosswinds on the source noise radiation characteristics have not been thoroughly investigated.

It is the objective of this paper to assess the effects of crosswind flight on the noise generation of helicopter main rotors to first-order, using a semi-empirical model of the Bell 430 helicopter. These results are compared to noise measurements of the Bell 430 during no wind and crosswind flight conditions. Recommendations are then made for new flight testing procedures for routine source noise characterization with the aim of reducing the impact of winds on the measurements.

THEORY

The model applied in this paper to assess the effects of crosswind flight on main rotor harmonic noise radiation is an extension of a previously developed semi-empirical model for estimating helicopter main rotor aerodynamics and acoustics. (Refs. 11,12) The model employs the Ffowcs Williams – Hawkings (FW–H) acoustic analogy method. (Ref. 13) Aerodynamic inputs are provided for each condition using a prescribed wake model combined with an incompressible indicial unsteady aerodynamics model. The FW–H equation is solved numerically using Farassat Formulation 1A. (Ref. 14) Acoustic sources off the blade surfaces, such as those causing High Speed Impulsive (HSI) noise, are neglected for the moderate advancing tip

Mach number range examined in this paper. Thickness noise is directly computed from the blade geometry and rotor operating condition. Loading noise, both lower harmonic and BVI noise, is determined from an assumed aerodynamic model adapted to measured data using the Fundamental Rotorcraft Acoustic Modeling from Experiments (FRAME) technique. (Ref. 15) Since FRAME is based on non-dimensional parameters, measured data can come from multiple sources; in this paper data from the $1/7^{th}$ scale Operational Loads Survey rotor tested in the DNW windtunnel (Ref. 16) is combined with flight test data from the Bell 430 helicopter collected during a NASA/Bell Helicopter/US Army flight test at Eglin Air Force Base in June 2011. (Ref. 17)

The wake model is based on the Beddoes prescribed wake, (Refs. 18, 19) but is modified to include additional dependent parameters adjusted by FRAME in order to adapt the model to existing empirical data for a particular rotor configuration. These additional parameters describe the non-uniform longitudinal and lateral inflow variations across the rotor disk, the initial vortex core size and its rate of growth (Ref. 20), the tip vortex rollup radius, the rate of wake contraction (Ref. 21), and the harmonic variation of vortex circulation strength about the rotor azimuth. The velocities induced by the wake onto the rotor blades are then corrected using the Beddoes-Leishman indicial aerodynamics model (Refs. 22, 23) to account for the delayed response of the shed wake on the rapidly changing aerodynamic loading felt by the blade elements. This is similar to the analytical modeling used in previous theoretical research into BVI noise, (Ref. 24) but with additional physically meaningful wake distortion terms to allow the model to be accurately fitted to the measured acoustic data. The corresponding rotor flap response is solved numerically under a rigid blade assumption.

This model is extended to crosswind flight conditions by incorporating a full six degree of freedom force and moment balance to establish the free flight trim condition of the entire helicopter during steady sideslipped flight. The mean main rotor forces and moments are calculated from blade element theory using the FRAME prescribed wake to compute the induced velocities; the tail rotor forces are computed under the assumption of uniform inflow with the tail rotor tip-path-plane angle of attack assumed equal to the fuselage sideslip angle. A non-linear least-squares numerical solver is used to find the main rotor cyclic and collective blade pitch, tail rotor collective blade pitch, and fuselage roll and pitch angles required to balance all forces and moments for the entire helicopter in steady flight.

An important consideration in this model is the effect of changing wind direction on the fuselage aerodynamic characteristics. Empirical data describing the fuselage moment, drag, lift, and side forces as a function of angle of attack and angle of sideslip are used in this model. The fuselage of the Bell 430 helicopter investigated in this paper was derived from that of the Bell 222 helicopter. Detailed aerodynamic data was collected for a full scale Bell 222 fuselage, including empennage, in the NASA Ames 40'x80' wind tunnel and is described by Squires in Reference 25. Of particular importance is the
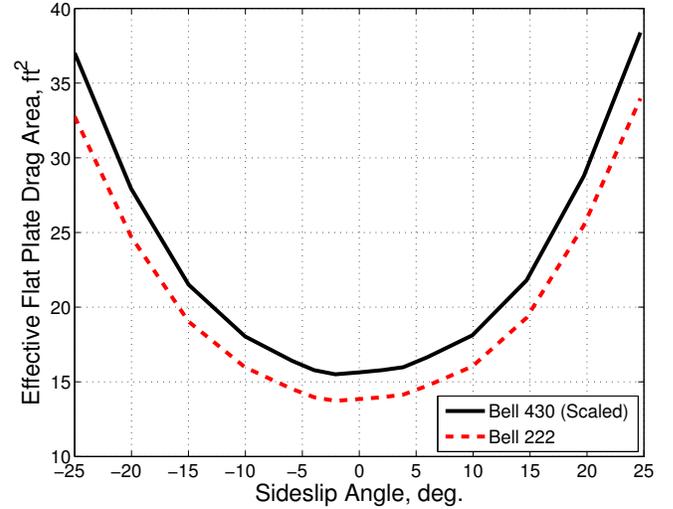
Fig. 3. Fuselage drag variation with sideslip angle for the Bell 430 derived from full scale measurements of the Bell 222 helicopter in the Ames 40'x80' wind tunnel. (Ref. 25)

change in fuselage drag due to a change in fuselage sideslip angle, as this strongly influences the rotor's tip-path-plane angle of attack with respect to the free stream velocity, and hence BVI noise. Following Schmitz, (Ref. 26) the angle of attack of the tip-path-plane resulting from an "X-force" balance in the aerodynamic axis system can be expressed to first order as:

$$\alpha_{TPP} \simeq \frac{-D_F - H}{W} - \gamma - \frac{1}{g}\left|\frac{dV_{GND}}{dt}\right|_x \tag{1}$$

where the fuselage drag is represented by:

$$D_F = \frac{1}{2}\rho V^2 f_e(\alpha_F, \beta_F) \tag{2}$$

The Bell 430 fuselage has a slightly higher drag than that of the Bell 222 at zero sideslip, but extensive data are not available; instead, the comprehensive Bell 222 fuselage aerodynamics data are uniformly scaled up to values more representative of the Bell 430 for use in this paper. Figure 3 shows the scaled-up variation in the effective flat plate drag area as a function of fuselage sideslip angle; as the sideslip angle of the fuselage increases beyond $5°$, a significant increase in the effective flat plate drag area of the fuselage is observed.

There are numerous trim solutions for steady flight in the presence of a crosswind. In this paper, two distinct trim conditions are considered and are shown Figure 4. In one, the pilot flies the helicopter with the fuselage aligned in the inertial flight path direction at the airspeed indicated by the non-swiveling pitot probe along the flight path direction. In this trim condition, the crosswind component of the wind velocity results in an aerodynamic sideslip angle of the fuselage, β_F. The fuselage produces a drag force, D_F, in the same direction as the free stream velocity, V. In addition, a fuselage side force, Y_F is generated normal to the free stream velocity vector, due to the sideslip angle of the fuselage. The pilot compensates for this side force by tilting the helicopter at a slight roll angle.
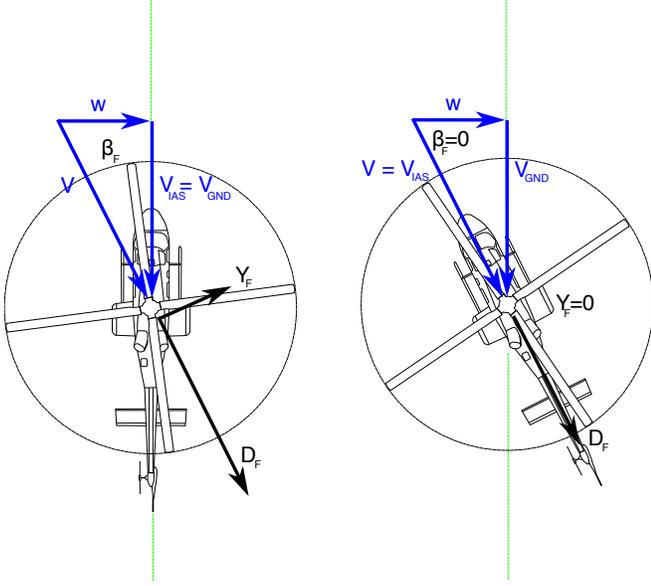
Fig. 4. Top view schematic of helicopter fuselage velocities and forces under crosswind conditions for a) sideslipped flight and b) "crabbed" flight.
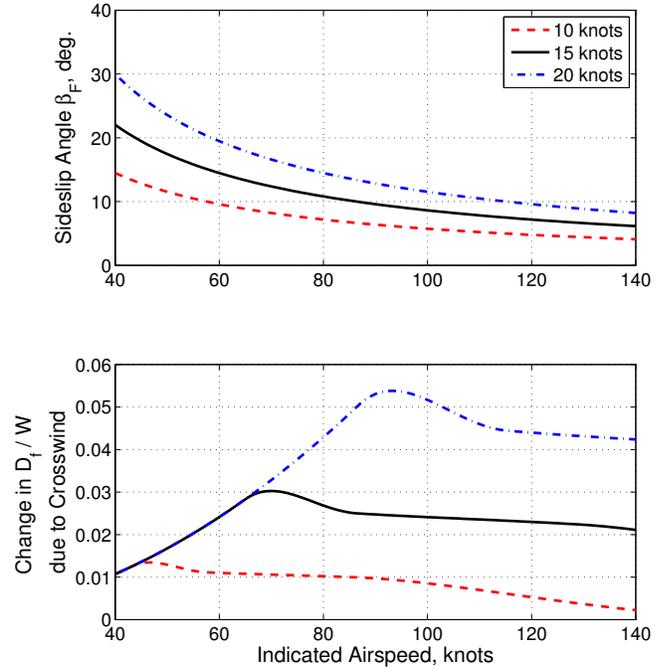
Fig. 5. Change in sideslip angle, β_F, and drag-to-weight ratio, D_f/W, as a function of airspeed, V_{IAS}, due to crosswinds of different magnitudes during sideslipped flight.

Equation 3 describes the increase in main rotor advance ratio seen by the rotor caused by the introduction of the crosswind during sideslipped flight. Main rotor BVI noise is a strong function of advance ratio; however, for realistic indicated airspeeds and wind velocities, the change in the advance ratio due to the crosswind is slight. For example, the introduction of a 15 knot crosswind will cause an increase in the advance ratio by about 1.5% over the no wind condition when flying 80 knots indicated airspeed in sideslipped flight.

$$\Delta\mu = \frac{\sqrt{V_{IND}^2 + w^2} - V_{IND}}{\Omega R} \tag{3}$$

In the second trim condition, the pilot flies with the helicopter fuselage "crabbed" to align with the free stream velocity vector resulting in zero aerodynamic sideslip of the fuselage. The fixed pitot probe now indicates the free stream velocity of the aircraft, resulting in the same main rotor advance ratio as the no wind condition. Because the fuselage is laterally symmetric, the fuselage side force, Y_F, approaches zero in this trim condition and the fuselage drag force reaches a minimum. Under both trim conditions, the crosswind skews the free stream velocity relative to the initial flight path by an angle β_I, such that:

$$\sin\beta_I = \frac{w}{V} \tag{4}$$

Flying sideslipped in a crosswind could have a significant impact on the rotor angle of attack, depending on the airspeed of the helicopter and the magnitude of the wind. Figure 5 plots the fuselage aerodynamic sideslip angle and the change in the drag-to-weight ratio relative to flight in no wind conditions for the Bell 430 helicopter in sideslipped flight at various airspeeds and crosswind magnitudes. From Equation 1, it is clear that the drag-to-weight ratio, D_f/W, has a strong effect on the angle of

attack of the main rotor tip-path-plane with respect to the free stream velocity, which could result in significant changes in the magnitude of BVI noise. At low flight speeds, the fuselage sideslip angle will be high; however, because the free stream velocity is low, fuselage drag forces are small. At high flight speeds, the fuselage drag forces are high but the sideslip angle is low; at low sideslip angles, the fuselage drag characteristics are relatively insensitive to small changes in the sideslip angle, as can be seen in Figure 3. However, at moderate airspeeds, the fuselage sideslip will result in a significant change in the drag-to-weight ratio of the helicopter, resulting in a larger change in the tip-path-plane angle of attack relative to no wind conditions.

Wind Gradients In practice, the wind speed is not constant during a descending flight condition; the wind speed approaches zero near the ground and increases with increasing altitude. For a helicopter descending at a constant airspeed in a varying headwind, this results in an acceleration in the inertial frame, changing the trim of the helicopter. For example, assuming a linear wind gradient, $w(h) = \xi \cdot h$, the inertial acceleration of a descending helicopter is:

$$\left|\frac{dV_{GND}}{dt}\right|_x = \frac{dV_{GND}}{dt} = V\xi\sin\gamma \tag{5}$$

To first order, this can be related to the change in the tip-path-plane angle of attack through Equation 1, i.e.

$$\Delta\alpha_{TPP} \simeq -\frac{V\xi}{g}\sin\gamma \tag{6}$$

4

The effect of a crosswind gradient on the trim of the helicopter depends on the piloting technique. When the pilot flies with the fuselage aligned with the inertial flight path direction, the indicated airspeed is not affected by the wind blowing across the flight path. Consequently, the helicopter does not accelerate in the inertial frame, although there is a gradual change in the magnitude and direction of the wind seen by the rotor. As the helicopter approaches the ground, the flight condition becomes more like that of the zero wind case.

When the pilot "crabs" the fuselage such that the fuselage is aligned with the free stream velocity (i.e. zero sideslip), the indicated airspeed reflects the magnitude of the free stream velocity and is somewhat affected by the crosswind. As the pilot maintains a constant indicated airspeed, the helicopter will accelerate along the flight path direction due to the changing crosswind magnitude. For a crosswinds less than the free stream velocity, the resulting acceleration along the flight path direction is:

$$\frac{dV_{GND}}{dt} = -\frac{w}{\sqrt{V^2 - w^2}}\frac{dw}{dt} \qquad (7)$$

This acceleration may be resolved along the free stream velocity direction, resulting in:

$$\left|\frac{dV_{GND}}{dt}\right|_x = -\frac{w}{V}\frac{dw}{dt} \qquad (8)$$

For a linear wind gradient, this results in a non-constant change in the tip-path-plane angle of attack of:

$$\Delta\alpha_{TPP} \simeq -\frac{w}{V}\frac{V\xi}{g}\sin\gamma = -\frac{w\xi}{g}\sin\gamma \qquad (9)$$

Under realistic flight conditions, where the crosswind magnitude is much smaller than the free stream velocity, this indicates that the change in the longitudinal trim of the helicopter due to a wind gradient will also be much less for the crosswind case than for a headwind or tailwind.

EFFECTS OF CROSSWINDS ON MEASURED DATA

During the Bell 430 flight test at Eglin AFB, noise measurements were captured for several test points under a range of wind conditions; these data were used to construct acoustic hemispheres for use in acoustic mission planning tools such as RNM. Figure 6a shows the Lambert projection of the Blade-Vortex Interaction Sound Pressure Level (BVISPL) contours for the Bell 430 on the surface of a hemisphere set six rotor diameters away from hub during a steady 80 KIAS, -7.5° descent flight condition with near zero winds. In this paper, the BVISPL metric is defined as the unweighted sum of all noise from the 6th to the 40th harmonics of the main rotor blade passing frequency. High levels of BVI noise are radiated ahead of and below the helicopter during this descending flight condition.

During the test program, this flight condition was repeated in the presence of a 11 knot crosswind coming from the advancing side of the flight path. Figure 6b shows the measured

BVISPL hemisphere for the Bell 430 helicopter captured during an 80 KIAS, -7.5° flight path angle condition in the presence of a steady crosswind of approximately 11 knots at flight altitude blowing nearly orthogonal to the flight track from the advancing side. This results in a skew angle between the inertial flight path and the aerodynamic velocity seen by the rotor, β_I, of about 8°. Inflight instrumentation measured the aerodynamic sideslip of the fuselage throughout the run; for most of the descent, the pilot kept the fuselage "crabbed" with low sideslip angles not exceeding 5°. However, as the vehicle approached the ground near the end of the descent, the sideslip angle tended to increase as the pilot aligned the fuselage with the flight path—by this time, the helicopter had passed the microphone array and the rear portion of the hemisphere was measured where lower levels of rotor harmonic noise are radiated. In comparison to the data collected for the same condition in near-zero winds (Fig. 6a), there is little change in the BVI noise radiation except that the "directivity" has been yawed towards the advancing side. Unfortunately, measured data was not collected for this flight condition at higher sideslip angles.

Data were also collected for higher speed level flight conditions, where no significant BVI noise occurs but higher levels of lower harmonic noise are radiated. Figure 7a shows the OverAll Sound Pressure Level (OASPL) hemispheres captured for the helicopter in a 130 KIAS level flight condition in a steady 4 knot tailwind. Noise is radiated ahead of the helicopter near the plane of the rotor and towards the advancing side.
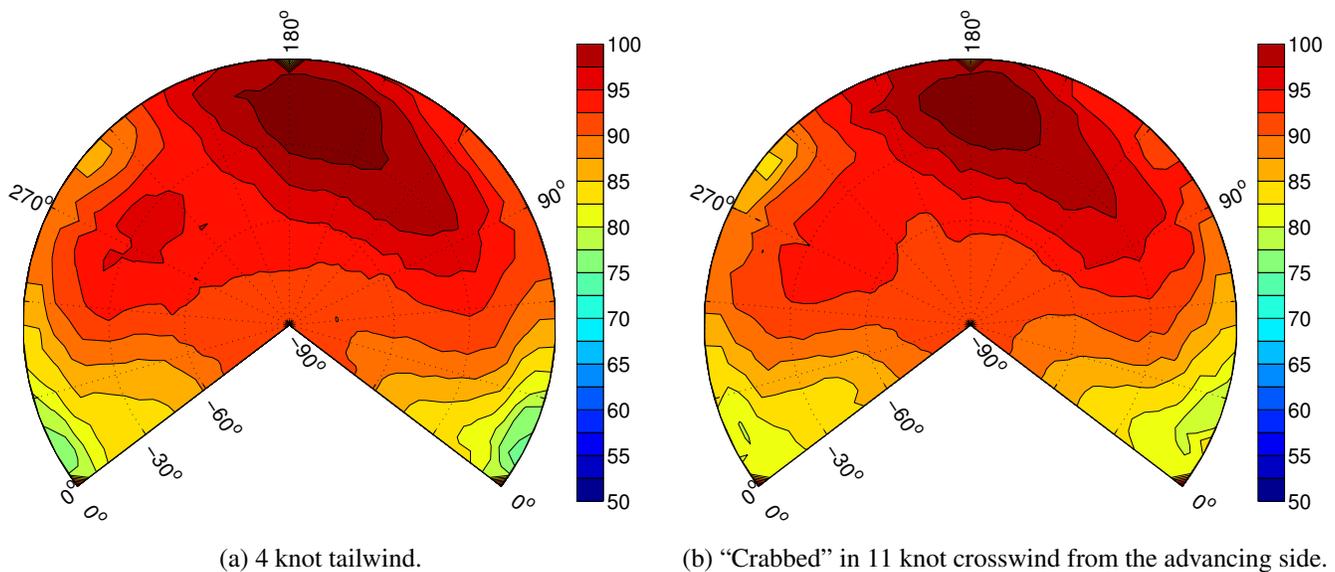
The same condition was flown in a 11 knot crosswind from the advancing side of the flight path. The measured acoustic hemisphere OASPL contours are shown in Figure 7b. Once again, the pilot flew with the fuselage oriented for low sideslip; the measured sideslip angle was generally below 3° throughout the run. However, the skew angle between the inertial flight path and the aerodynamic velocity, β_I, is only 6° because of the higher flight speed of the helicopter. The change in noise radiation relative to the hemisphere for low wind conditions, Figure 7a, is slight and well within normal measurement variability.

BELL 430 MODEL VALIDATION

The BVISPL contours predicted by the semi-empirical FRAME model of the Bell 430 helicopter are shown for the 80 KIAS, -7.5° flight path angle (FPA) condition with no wind in Figure 8a. The levels and directivity of BVI noise compare well with the measured data for the same flight condition shown previously in Figure 6a. The FRAME model is applicable over a range of flight conditions. Figure 9 compares the model predicted results to BVI noise radiated directly ahead of the helicopter and 30° below the horizon across a range of flight path angles to the measured BVISPL values; the model agrees well with the measured data during the steeper descent conditions where BVI dominates the BVISPL metric. At the shallower 0° and 3° flight path angles, the measured values exceed the prediction; note that the tail rotor noise is not modeled in the prediction but is included in the measured data. The tail rotor contributes significantly to noise in the BVISPL

(a) No wind.

(b) 11 knot crosswind from the advancing side.
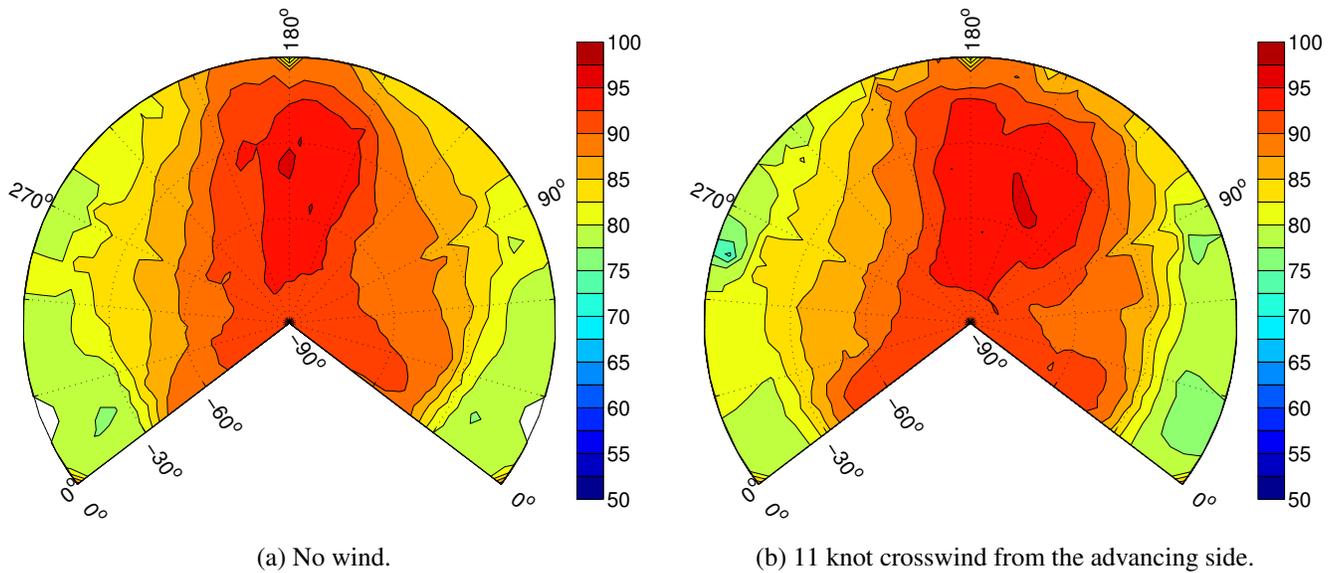
Fig. 6. Measured BVI noise hemispheres for 80 KIAS, -7.5° FPA flight condition, dB BVISPL

(a) 4 knot tailwind.

(b) "Crabbed" in 11 knot crosswind from the advancing side.

**Fig. 7. Measured noise hemispheres for 130 KIAS, level flight, dB OASPL.**

frequency range because the tail rotor blade passing frequency is about three times higher than that of the main rotor.

The model can be applied to look at the effects of crosswinds on noise radiation. Figure 8b shows the BVISPL contours for the helicopter in the same descending flight conditions, but with a steady 15 knot crosswind from the advancing side of the helicopter. The helicopter has been trimmed to "crab" the fuselage. The BVI noise radiation is unchanged in magnitude, but now radiates more towards the advancing side of the flight path, as was observed in the measured data for "crabbed" flight in crosswinds shown in Figure 6b.

In addition to BVI, the model can be applied to look at lower harmonic loading and thickness noise. Figure 10a shows

the OASPL contours predicted by the main rotor noise model trimmed for the Bell 430 in 130 KIAS level flight in no wind conditions. The model output exhibits fairly good agreement with the measured noise hemisphere shown in Figure 7a.

Figure 10b shows the same flight condition trimmed with the fuselage "crabbed" for zero sideslip in the presence of a steady 15 knot wind from the advancing side of the flight path. Very little change in noise radiation is observed; there is a slight shift in the directivity 7° to towards the advancing side. This is similar to the effect of the crosswind on the measured data for 130 KIAS flight that was shown in Figure 7b.
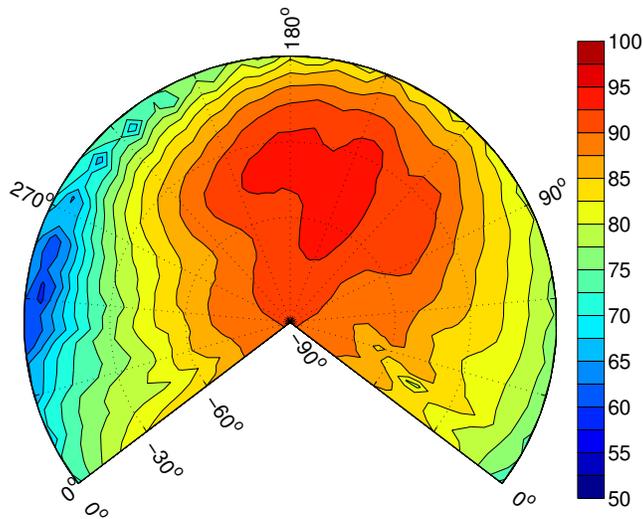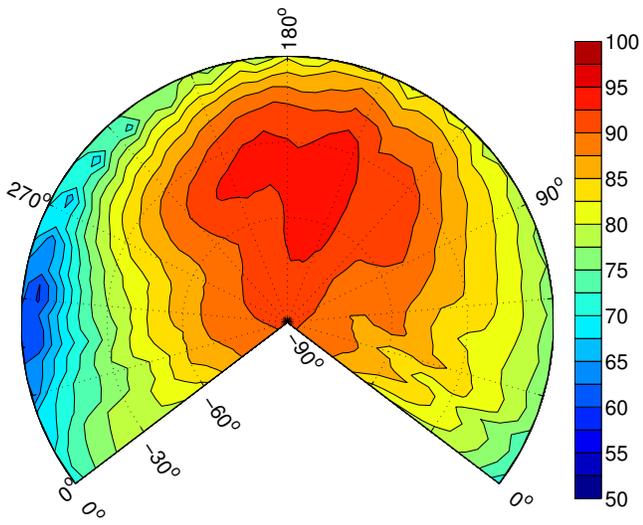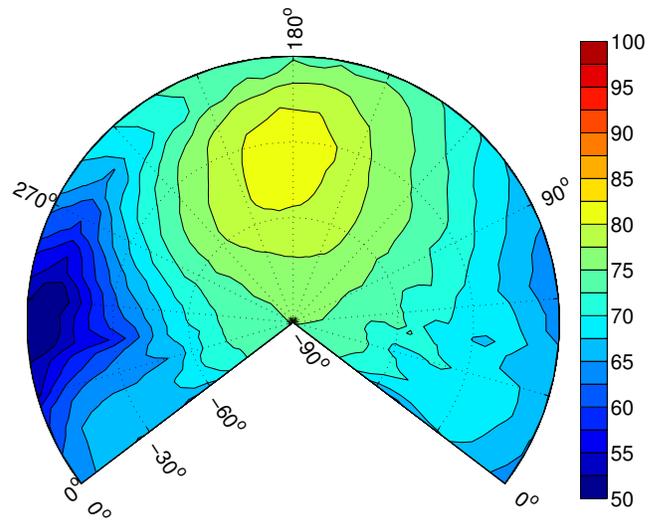
(a) No wind.
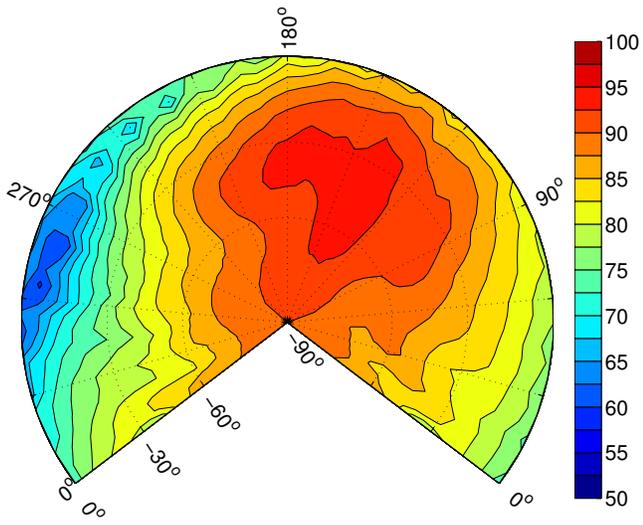
(b) "Crabbed" in 15 knot crosswind from the advancing side.
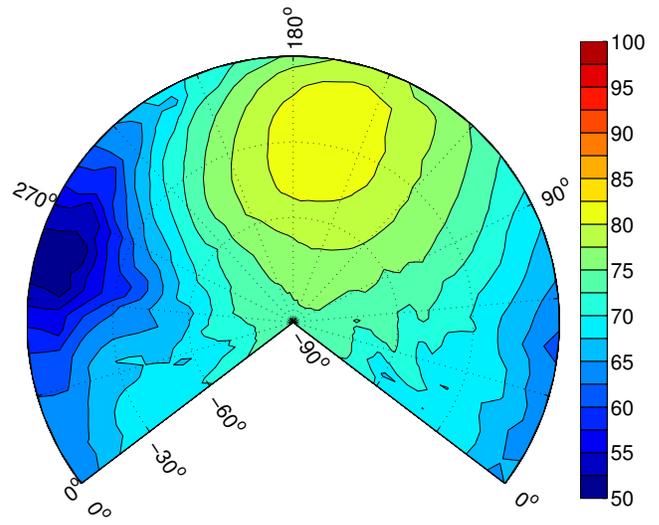
(c) Sideslipped in 15 knot crosswind from the advancing side.

(d) "Crabbed" in 15 knot crosswind from the retreating side.

(e) Sideslipped in 15 knot crosswind from the retreating side.

Fig. 8. Predicted BVI noise hemispheres for 80 KIAS, -7.5° FPA flight, dB BVISPL.

RESULTS AND DISCUSSION

Effects of Piloting Technique and Wind Direction

In addition to estimating the noise radiation in low wind and "crabbed" crosswind flight, the model can be trimmed to a sideslipped flight condition to examine the effect of piloting technique on crosswind noise radiation. Figure 8c shows the horizon-fixed noise hemisphere for the same 80 KIAS, -7.5° FPA flight condition (Fig. 8a) where the pilot has trimmed the fuselage to align with the flight path in the presence of a steady 15 knot crosswind coming from the advancing side of the flight path. The presence of the crosswind causes the fuselage to operate in a 10° aerodynamic sideslip, increasing the drag force by about 15% over the "crabbed" condition. In addition, a small lateral side force towards the advancing side is generated. The change in fuselage drag forces causes the rotor to tilt farther forward and towards the advancing side than in the no wind condition. The change in rotor trim results in a decrease in the tip-path-plane angle of attack by about 2°. This causes in a decrease in BVI noise relative to no wind conditions, with the peak BVISPL about 11 dB lower than that of either the no wind (Fig. 8a) or "crabbed" (Fig. 8b) flight conditions. A reduction in noise levels is observed because the highest BVI noise levels are observed in no wind conditions at a -7.5° flight path angle for the Bell 430 at 80 KIAS (Fig. 9). For a steeper descent, the decrease in tip-path-plane angle of attack due to sideslipped flight could result in an increase in BVI noise.

In addition to a change in the tip-path-plane angle of attack, the increase in lateral side force causes the rotor tip-path-plane to roll 5° towards the advancing side along the aerodynamic free stream velocity vector—this has little impact on the noise generation, but does cause the directivity of the radiated noise to roll slightly towards the advancing side along with the tip-path-plane. Lastly, because the directivity of the radiated noise is determined by the motion of the rotor with respect to the medium, irrespective of the inertial flight path of the vehicle, the noise radiation is yawed along with the free stream velocity vector towards the advancing side of the flight-path oriented hemisphere. This directivity shift is similar to that observed for "crabbed" flight, shown previously in Figure 8b.

Figure 8d shows the acoustic hemisphere contours predicted by the model for the same flight condition where the pilot has "crabbed" the fuselage in response to a steady 15 knot crosswind now coming from the retreating side. The aerodynamic flight condition is indistinguishable from the flight condition in no wind conditions (Fig. 8a), but is now shifted towards the retreating side because of the change in the crosswind direction. Likewise, the effects of sideslipped flight in a crosswind from the retreating side, shown Figure 8e, are similar to those due to sideslipped flight due to winds from the advancing side (Fig. 8c). The sideslip caused by the wind from the retreating side causes a nearly identical decrease in the main rotor-tip-path plane angle of attack as was caused by the wind from the advancing side, however the rotor is now rolled further towards the retreating side. Of course, the noise radiation pattern is
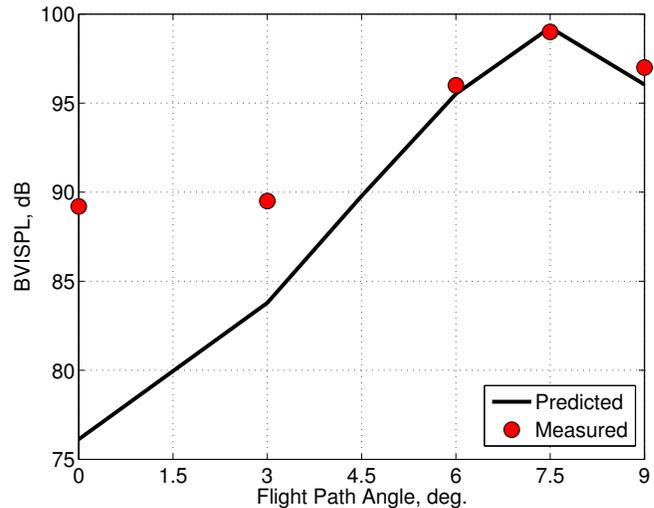
Fig. 9. Comparison of measured and predicted BVISPL at 180° azimuth, -30° elevation at 80 KIAS for various flight path angles.

also yawed towards the retreating side, as was also observed for "crabbed" flight in the same winds.

In all cases, the introduction of the crosswind causes a shift in the directivity of radiated noise towards the incoming wind direction. During sideslipped flight, when the pilot keeps the fuselage aligned with the inertial flight path, the increase in drag results in significant changes in BVI noise. However, when the pilot "crabs" the fuselage for zero sideslip, the BVI noise state is unchanged. Therefore, it seems favorable to fly the helicopter in a "crabbed" trim condition to minimize the impact of winds on the acoustic state of the vehicle during noise characterization measurements.

Effects of Crosswinds at Different Airspeeds

The effect of the crosswinds on the trim state of the rotor will be strongly dependent on the flight speed of the vehicle. At lower flight speeds, the same crosswind will cause a greater difference in orientation of aerodynamic and inertial velocity vectors of the rotor; conversely, at lower flight speeds the fuselage aerodynamic forces are smaller and their effects on the trim of the helicopter generally reduced. Figure 11a shows an acoustic BVISPL hemisphere for a slower 50 KIAS -7.5° FPA flight condition without wind. As would be expected, the BVI noise levels are somewhat reduced from the higher speed flight condition. The change in rotor advance ratio has also cause the predominate BVI to be radiated more towards the retreating side of the rotor than for the higher speed case.

Figure 11e shows the acoustic hemisphere for the corresponding flight condition in a 15 knot crosswind from the retreating side where the fuselage is oriented along the flight path direction. This results in a fuselage sideslip angle of about 15°. There is a small reduction of about 2 dB in the peak BVI

(a) No wind.

(b) "Crabbed" in 15 knot crosswind from the advancing side.

(c) Sideslipped in 15 knot crosswind from the advancing side.
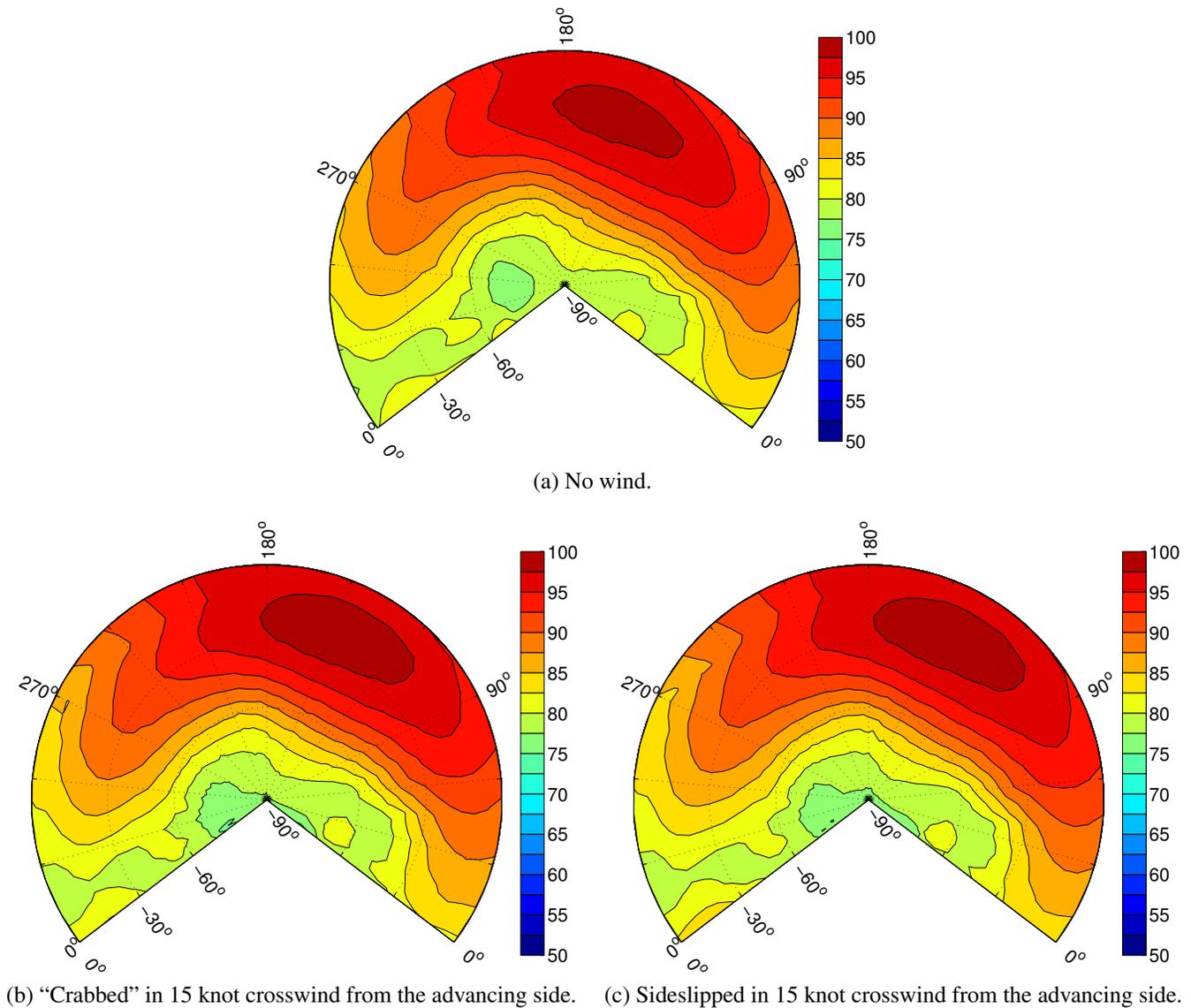
**Fig. 10. Predicted overall noise hemispheres for 130 KIAS level flight, dB OASPL.**

noise level relative to no wind conditions caused by a reduction in the tip-path-plane angle of attack by about $1°$. Figure 11c shows the sideslipped condition with the crosswind approaching from the advancing side of the flight path, with a similar reduction in BVI noise levels. In both cases, the directivity is yawed with respect to the flight path due to the crosswind.

Figures 11d and 11b show the effects of the 15 knot crosswind from the retreating and advance sides, respectively, for the helicopter when the fuselage is "crabbed" for zero sideslip. As in the higher speed case, the only significant change in radiated noise is a shift in the directivity following the change in the aerodynamic velocity direction with respect to the inertial flight path direction.

In higher speed level flight conditions, significant BVI does not occur and the lower harmonic noise sources are most significant. Figure 10c shows the OASPL contours for the 130 KIAS level flight condition in a 15 knot crosswind blowing from the advancing side of the flight path, where the pilot has

aligned the fuselage in the flight path direction inducing a $4°$ aerodynamic sideslip of the fuselage. The small sideslip angle results in a change of the tip-path plane angle of attack by about $1.5°$ which does not have much effect on the lower harmonic loading noise sources. The primary result of the crosswind is a shift in the directivity of the radiated noise towards the advancing side of the flight path by about $7°$. This can be compared to the same condition where the pilot "crabs" the fuselage for zero sideslip (Fig. 10b) producing nearly identical OASPL contours with no change in the rotor angle of attack relative to no wind conditions.

In general, larger directivity changes are observed at lower airspeeds than at higher airspeeds for the same crosswind. This is because the skew angle between the inertial and aerodynamic velocities, β_I, is greater when the helicopter is flying at a lower speed. However, during sideslipped flight the effect of fuselage sideslip on the rotor trim state, and hence BVI noise, is reduced at lower speed even though the aerodynamic sideslip angle of
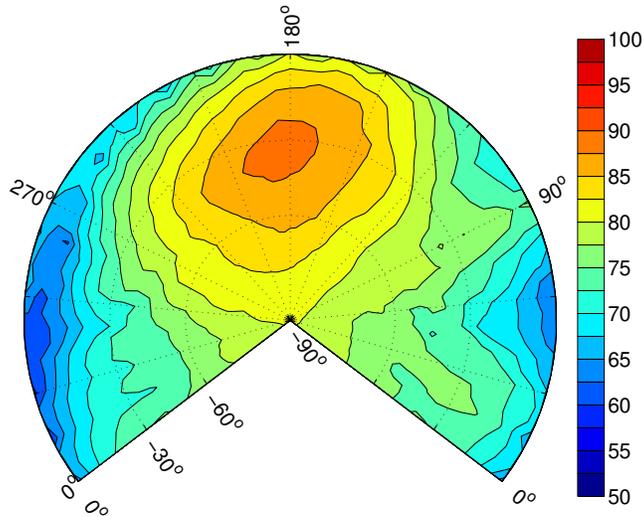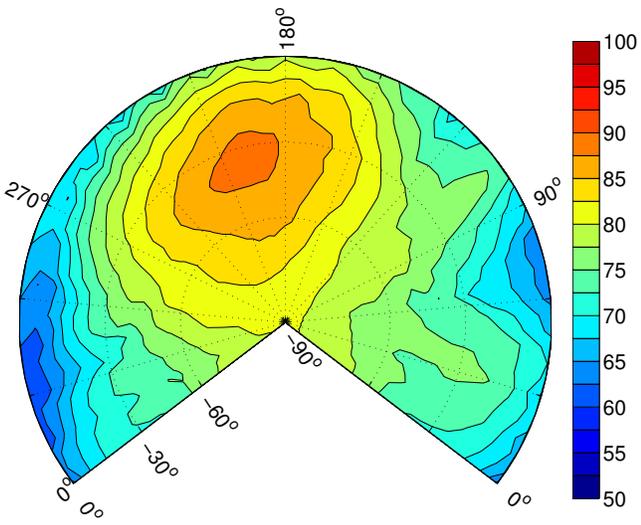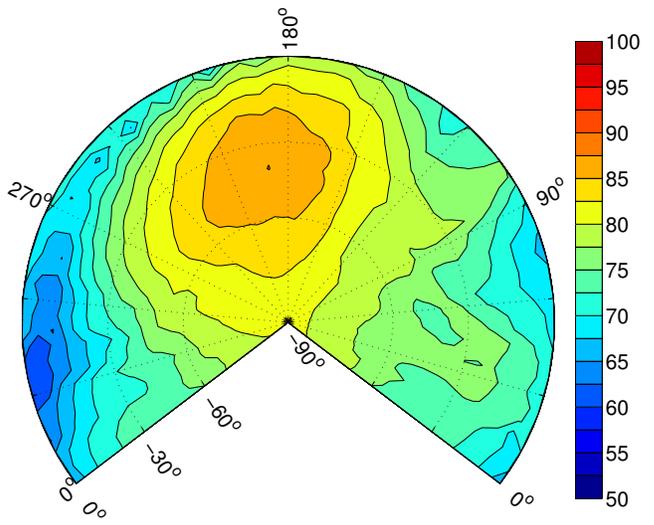
(a) No wind.
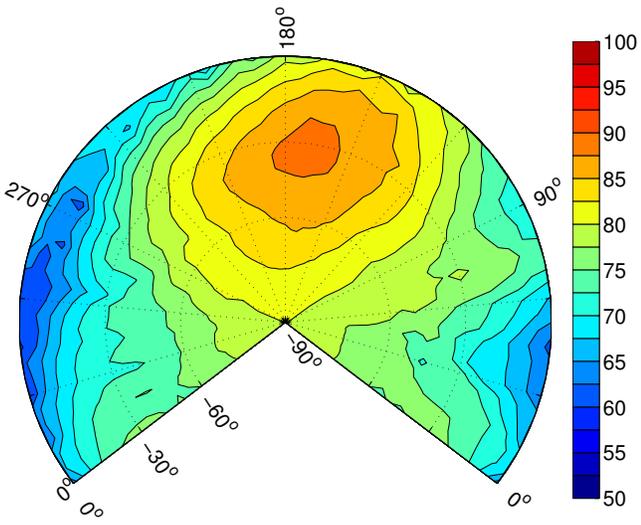
(b) "Crabbed" in 15 knot crosswind from the advancing side.
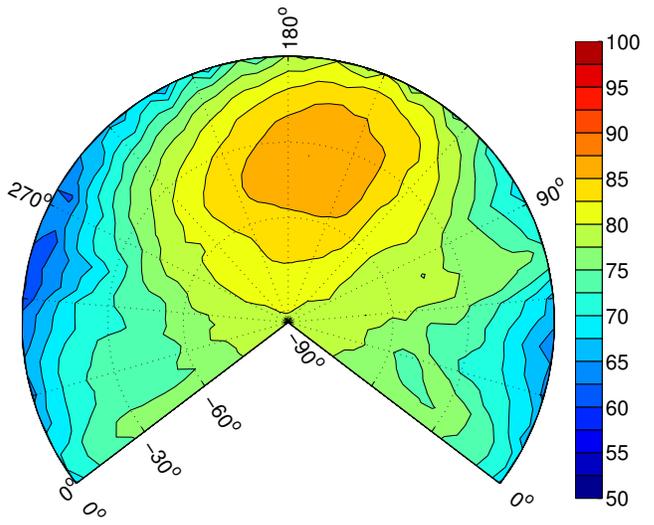
(c) Sideslipped in 15 knot crosswind from the advancing side.

(d) "Crabbed" in 15 knot crosswind from the retreating side.

(e) Sideslipped in 15 knot crosswind from the retreating side.

Fig. 11. Predicted BVI noise hemispheres for 50 KIAS, -7.5° FPA flight, dB BVISPL.

the fuselage has increased. This is because the fuselage drag increases with the square of the aerodynamic velocity, and has little effect on the rotor trim at low flight speeds. At high speed, crosswinds have little impact on the dominant lower harmonic noise sources because the skew angle β_I is quite small. Likewise, there is little difference between the "crabbed" and sideslipped piloting techniques at high speed.

Effects of Wind Gradients

As discussed earlier, wind gradients are known to have a strong effect on BVI noise radiation when the prevailing wind direction is aligned with the flight path direction. Figure 12a shows the BVISPL hemisphere for a helicopter operating in a 80 KIAS, -7.5° flight condition in the presence a headwind with a linear wind gradient of 15 knots at 300 feet altitude to zero knots at ground level, this corresponds to a decrease of the tip-path-plane angle of attack of about 2° from the no wind condition shown previously (Fig. 8a). Relative to the no wind condition, the peak BVI noise has been reduced by about 9 dB.

Figure 12b shows the BVISPL hemisphere for a helicopter in the same flight condition in the presence of the same wind gradient, this time aligned so that wind blows from the retreating side of the flight path. The helicopter's fuselage is "crabbed" for zero sideslip and is at a 300 foot altitude, such that the wind magnitude is 15 knots. This results in a decrease in the tip-path-plane angle of attack of about 0.35° from the no wind condition (Fig. 8a) and a reduction in the peak BVISPL by about 1 dB. No acceleration is imparted by the wind gradient when the helicopter is flown with the fuselage aligned with the flight path–in this case, the BVI noise radiation characteristics will be identical to the sideslipped case for a steady 15 knot crosswind (Fig. 8e).

Overall, the effects of wind gradients on BVI noise generation are much larger when prevailing winds are oriented along the flight path than when they are oriented across the flight path. From Equations 6 and 9, it is expected that the acceleration imparted when flying a constant airspeed descent in winds will be much less for "crabbed" flight in a crosswind gradient than in a head or tailwind gradient. For low to moderate crosswinds, effects of wind gradients on noise generation can be neglected when flying "crabbed." When flying sideslipped along the inertial flight path direction, no accelerations are imparted when descending in a crosswind wind gradient, although the sideslip still has a significant aerodynamic effect on the trim of the helicopter.

CONCLUSIONS

Crosswind flight has two effects on rotor harmonic noise generation. First, the introduction of the crosswind changes the orientation of the aerodynamic velocity vector with respect to observers on the ground. Second, the crosswind may affect the trim state of the helicopter and rotor, depending on how the helicopter is piloted. Using an analytical model of the Bell 430, the noise radiated under different wind conditions was assessed leading to the following conclusions:

- Blade-vortex interaction noise, produced at low-to-moderate airspeeds, is highly influenced by the pilot's choice of trim during crosswind flight. If the fuselage is aligned with the flight path, increases in the drag of the fuselage can lead to significant changes in the angle of attack of the rotor tip-path-plane with respect to the aerodynamic velocity, causing changes in the magnitude of BVI noise radiated by the helicopter. If the pilot trims the helicopter for zero fuselage sideslip, "crabbing" the fuselage with respect to the flight path, the change in the trim state of the rotor is minimal.

- The change in trim state due to fuselage sideslip could be exploited by the pilot to reduce noise, e.g. by intentionally sideslipping the helicopter during a shallow descent condition to decrease the rotor tip-path-plane angle of attack and reduce BVI noise. Conversely, sideslipping the helicopter during a steep descent could result in an increase in BVI noise.

- Crosswinds have little effect on the magnitude of lower harmonic noise radiation, typically measured at higher flight speeds, since these noise sources are relatively insensitive to the trim condition of the rotor.

- While steady head or tail winds have no effect on the rotor's acoustic state, in reality, wind gradients cause a significant change in the rotor trim during descending flight conditions where BVI occurs. The effects of wind gradients on BVI noise radiation are much less when winds are oriented across the flight path.

- In all cases, the change in the direction of the aerodynamic velocity seen by the rotor causes the directivity of radiated noise to rotate towards the wind direction, with respect to the ground-based observers.

Implications for Acoustic Flight Tests

These conclusions lead to the following recommendations for flight test procedures for helicopter noise source characterization:

- The flight path should be oriented such that the prevailing winds are across the flight path, because the effects of crosswinds and crosswind gradients on noise generation at the source are slight. During descending flight, headwind or tailwind wind gradients have greater effects on noise generation at the source than crosswind gradients. In addition, propagation effects are known to be much greater when the direction of propagation is along or against the prevailing wind direction. In crosswind flight, the propagation from the helicopter to the microphone array will be primarily oriented across the prevailing wind direction, minimizing the effects of wind on the noise measurement.

- The pilot should "crab" the fuselage to maintain coordinated zero sideslip flight when there are crosswinds and

(a) Headwind gradient.   (b) Crosswind gradient.
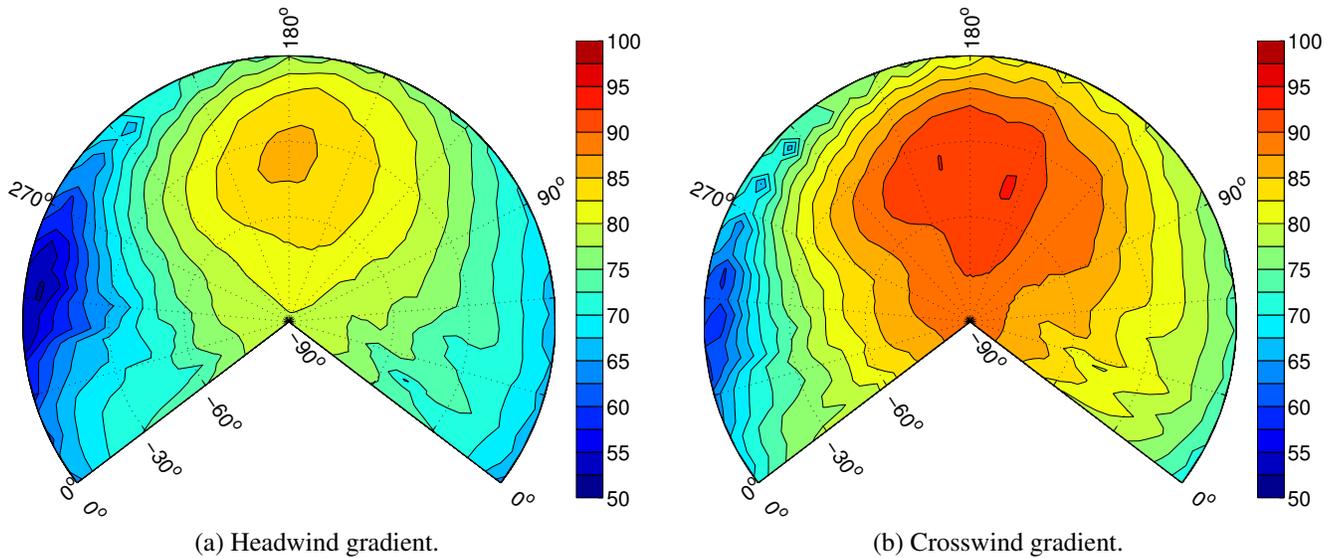
Fig. 12. Predicted BVI noise hemisphere for 80 KIAS, -7.5° FPA flight in a wind gradients, dB BVISPL.

avoid aligning the fuselage with the ground reference, especially as altitude decreases.

- Even when flying in crosswinds, descending "approach" conditions should be flown during low wind conditions. Higher speed level flight "cruise" conditions may be flown in higher wind speeds as they are less sensitive to changes in trim and because the same crosswind will result in a smaller shift in directivity at higher speeds.

ACKNOWLEDGEMENTS

REFERENCES

[1] Lucas, M. J. and Marcolini, M. A., "Rotorcraft Noise Model," AHS Technical Specialists' Meeting for Rotorcraft Acoustics and Aerodynamics, October 1997.

[2] Conner, D. A. and Page, J. A., "A Tool for Low Noise Procedures Design and Community Noise Impact Assessment: The Rotorcraft Noise Model (RNM)," Heli Japan, 2002.

[3] Page, J. A., Wilmer, C., and Plotkin, K. J., "Rotorcraft Noise Model Technical Reference and User Manual," Technical Report WR 08-04, Wyle, February 2008.

[4] Snyder, J. P., "Map Projections: A Working Manual," Technical Report PP1395, USGS, 1982.

[5] Pridmore-Brown, D. C., "Sound Propagation in a Temperature- and Wind-Stratified Medium," *The Journal of the Acoustical Society of America*, Vol. 34, (4), 1962, pp. 438–443. doi: 10.1121/1.1918146

[6] Rasmussen, K., "Outdoor sound propagation under the influence of wind and temperature gradients," *Journal of Sound and Vibration*, Vol. 104, (2), 1986, pp. 321 – 335. doi: 10.1016/0022-460X(86)90271-3

[7] Wiener, F. M. and Keast, D. N., "Experimental Study of the Propagation of Sound over Ground," *The Journal of the Acoustical Society of America*, Vol. 31, (6), 1959, pp. 724–733. doi: 10.1121/1.1907778

[8] Sprague, M., Raspet, R., and Ostashev, V. E., "Crosswind effects on acoustic propagation," *The Journal of the Acoustical Society of America*, Vol. 94, (3), 1993, pp. 1872–1872. doi: 10.1121/1.407628

[9] Li, Y. L., White, M. J., and Franke, S. J., "New fast field programs for anisotropic sound propagation through an atmosphere with a wind velocity profile," *The Journal of the Acoustical Society of America*, Vol. 95, (2), 1994, pp. 718–726. doi: 10.1121/1.408431

[10] Sim, B. W., Schmitz, F. H., and Beasman, T., "Blade-Vortex Interaction (BVI) Noise of Helicopters Operating in Horizontal Wind Shear," American Helicopter Society 61st Annual Forum, May 2005.

[11] Greenwood, E. and Schmitz, F. H., "A Parameter Identification Method for Helicopter Noise Source Identification and Physics-Based Semi-Empirical Modeling," American Helicopter Society 66th Annual Forum, May 2010.

[12] Greenwood, E. and Schmitz, F. H., "The Effects of Ambient Conditions on Helicopter Rotor Source Noise Modeling," American Helicopter Society 67th Annual Forum, May 2011.

[13] Ffowcs Williams, J. E. and Hawkings, D. L., "Sound generation by turbulence and surfaces in arbitrary motion," *Philosophical Transactions of the Royal Society of London*, Vol. 264, May 1969, pp. 321–342.

[14] Farassat, F., "Derivation of Formulations 1 and 1A of Farassat," Technical Report TM-2007-214853, NASA, 2007.

[15] Greenwood, E., *Fundamental Rotorcraft Acoustic Modeling from Experiments (FRAME)*, Ph.D. thesis, University of Maryland, January 2011.

[16] Boxwell, D. A., Schmitz, F. H., Splettstoesser, W. R., and Schultz, K. J., "Helicopter Model Rotor-Blade Vortex Interaction Impulsive Noise: Scalability and Parametric Variations," *Journal of the American Helicopter Society*, Vol. 32, (1), 1987, pp. 3–12.
doi: 10.4050/JAHS.32.3

[17] Watts, M. E., Snider, R., Greenwood, E., and Baden, J., "Maneuver Acoustic Flight Test of the Bell 430 Helicopter," American Helicopter Society 68th Annual Forum, May 2012.

[18] Beddoes, T. S., "A Wake Model for High Resolution Airloads," International Conference on Rotorcraft Basic Research, February 1985.

[19] van der Wall, B. G., "The Effect of HHC on the Vortex Convection in the Wake of a Helicopter Rotor," *Aerospace Science and Technology*, Vol. 4, (5), 2000, pp. 321–336.

[20] Bhagwat, M. J. and Leishman, J. G., "Generalized Viscous Vortex Core Models for Application to Free-Vortex Wake and Aeroacoustic Calculations," 58th Annual Forum of the American Helicopter Society, June 2002.

[21] Landgrebe, A. J., "The Wake Geometry of a Hovering Helicopter Rotor and its Influence on Rotor Performance," *Journal of the American Helicopter Society*, Vol. 17, (4), 1972.

[22] Beddoes, T. S., "Practical Computation of Unsteady Lift," *Vertica*, Vol. 8, (1), 1984.

[23] Leishman, J. G., *Principles of Helicopter Aerodynamics*, Cambridge University Press, New York, second edition, 2006.

[24] Schmitz, F. H. and Sim, B. W.-C., "Radiation and Directionality Characteristics of Helicopter Blade-Vortex Interaction Noise," *Journal of the American Helicopter Society*, Vol. 48, (4), 2003, pp. 253–269.

[25] Squires, P. K., "Investigation of Correlation between Full-Scale and Fifth-Scale Wind Tunnel Test of a Bell Helicopter Textron Model 222," Technical Report CR-16662, NASA, 1982.

[26] Schmitz, F. H., "Reduction of Blade-Vortex Interaction (BVI) Noise through X-Force Control," *Journal of the American Helicopter Society*, Vol. 43, (1), 1998, pp. 14–24.
doi: 10.4050/JAHS.43.14